Estimation of enhanced electron density in the lower ionosphere using correlation between natural VLF emission intensity and CNA

Mitsunori Ozaki[1]*, Satoshi Yagitani[1], Isamu Nagano[2],
Hisao Yamagishi[3,4] and Natsuo Sato[3,4]

自然 VLF 放射強度と銀河雑音電波吸収（CNA）の相関関係を用いた
下部電離層電子密度の推定

尾崎光紀[1]*・八木谷聡[1]・長野　勇[2]・山岸久雄[3,4]・佐藤夏雄[3,4]

要旨:　本研究では，地上で観測される VLF ホイスラモード波（昼間に観測されるコーラス）の電離層減衰率と CNA を用いた新しい下部電離層電子密度のリモートセンシング技術を提案する．そのために，さまざまな電子密度モデルに対する両者の関係を理論的に評価している．評価の手法は，full-wave 解析を用いて VLF ホイスラモード波の下部電離層減衰率と CNA を理論計算している．計算結果は観測結果と同様に CNA と VLF 波動の負相関を示し，さらに，増大した電子密度モデルの最大電子密度高度が下がるにつれ，CNA-VLF 負相関の傾きが増大する関係を示した．つまり，観測された CNA-VLF 負相関の傾きが，降下粒子に伴う下部電離層を増大させる電子密度高度を推定する情報源に成りえるということが分かった．これは，夜間のみに生じる Trimpi 現象と共に，昼間の降下粒子検出に対する新しい下部電離層電子密度推定手法となるであろう．

Abstract:　In this study, we suggest a new remote sensing technique for enhanced electron density in the lower ionosphere by using the correlation between VLF whistler mode waves (daytime chorus emissions) and CNA, both observed on the ground. The ionospheric attenuations for VLF whistler mode and HF waves (as a CNA value) are calculated by using full-wave analysis to evaluate their correlations for various ionospheric electron density profiles enhanced by precipitating electrons. The calculation results show negative correlations between CNA and VLF whistler mode waves in accordance with the observation results. Then, the gradient of the negative correlation becomes larger with decreasing altitude of maximum electron density. Thus, we found that the correlation provides information on the vertical profile of the enhanced

[1]　金沢大学理工研究域電子情報学系．Institute of Science and Engineering, Kanazawa University, Kakuma-machi, Kanazawa 920-1192.

[2]　金沢大学．Kanazawa University, Kakuma-machi, Kanazawa 920-1192.

[3]　情報・システム研究機構国立極地研究所．National Institute of Polar Research, Research Organization of Information and Systems, Midori-cho 10–3, Tachikawa-City Tokyo 190-8518.

[4]　総合研究大学院大学複合科学研究科極域科学専攻．Department of Polar Science, School of Multidisciplinary Sciences, The Graduate University of Advanced Studies (SOKENDAI), Midori-cho 10–3, Tachikawa-City Tokyo 190-8518.

*　Corresponding author. E-mail: ozaki@reg.is.t.kanazawa-u.ac.jp

electron density in the lower ionosphere caused by electron precipitation. This allows the study of electron precipitation in the daytime, in addition to Trimpi events at nighttime.

1.   Introduction

Electron precipitation associated with pitch angle scattering by VLF emissions down to the polar region plays an important role in wave-particle interactions and particle energetics during substorms.   Considerable research on electron precipitation associated with natural VLF waves (whistler, chorus and hiss) has been conducted for several decades.   Rosenberg *et al.* (1971) found a correlation between VLF emissions observed at Siple station and X-ray bursts associated with precipitating particles (electron energy: 30 keV to 100 keV).   Hoffman and Laaspere (1972) reported that the occurrence of VLF hiss correlates well with precipitation events of low energy (0.7 keV) electrons from satellite observation.   Helliwell *et al.* (1973) reported one-to-one correlation between whistlers and Trimpi events from ground-based observation.   These events strongly indicate that VLF emissions dump energetic electrons into the ionospheric *D*-region (<95 km).   The electron density in the ionospheric *D*-region is altered by enhanced secondary ionization produced by these precipitating electrons. Thus, ground-based VLF remote sensing techniques are important for determining the electron density in the lower ionosphere (Cummer *et al.*, 1997).

On the other hand, medium energy (10 keV to 100 keV) electron precipitation has been investigated by riometers on the ground for several decades.   Cosmic radio noise in the HF range measured by a riometer exhibits stable daily variation in geomagnetic quiet periods.   However, it rapidly attenuates in a geomagnetic disturbance due to absorption in the ionospheric *D*-region, which has been abnormally ionized by the electron precipitation (Nielsen, 1980).   Thus, the cosmic radio noise absorption (CNA) measured by the riometer gives significant information about the medium energy electron precipitation down to the ionospheric *D*-region.   A good correlation between CNA measured by the riometer and medium energy electron precipitation has been reported in previous studies (*e.g.*, Jelly and Brice, 1967; Collis and Korth, 1985). Even though the riometer can be a useful ground-based instrument for investigating energetic particle precipitation, so far no one has investigated the altitude profile of enhanced ionization in the lower ionosphere.

In this study, we compare the CNA with the intensity of the VLF emissions, both observed in Antarctica, to find the correlation between them.   Then, we theoretically calculate the CNA and the attenuation of the down-going VLF whistler mode waves for various ionospheric models, and suggest that the CNA-VLF correlation gives information on the altitude extent of the enhanced ionospheric *D*-region.   Finally, we estimate the enhanced electron density in the *D*-region from the CNA and VLF observations and their theoretical by calculated values.

2.   VLF and CNA Observations in Antarctica

2. 1   Observation System

In this study, we used the ground-based observation data of natural VLF waves and of 30 MHz CNA both measured at West Ongul (69°01′S, 39°30′E, L-value: 6.2) in Antarctica.   Natural VLF waves were observed at West Ongul for the whole year of 2006.   A filter-bank type autonomous observation system of VLF magnetic fields was used to give continuous information on the North-South and East-West horizontal magnetic field intensities and its polarization in 4 spaced frequency channels (0.5, 1, 2, and 6 kHz), with time resolution of 0.5 second.   In this study, we focus on the 1 kHz channel measuring the intensity of polar chorus in the daytime.

The CNA at 30 MHz has been observed by a broad-beam riometer installed at West Ongul since 1981.   Its beam half-width is 60 degrees.   The riometer data are recorded in the digital format at the sampling rate of 20 Hz in the Upper Atmosphere Physics Monitoring system operated by the National Institute of Polar Research (NIPR), Japan.

2. 2   Correlation between 1 kHz Whistler Mode Wave Intensity and CNA

In order to find the relationship between the polar chorus and the CNA in polar region, we have compared the 1 kHz wave intensity with 30 MHz CNA observed in the daytime.   The observation data were smoothed with one-minute averaging to reduce the effect of impulsive noise such as spherics.   As an example, a typical event on 15 April, 2006 is shown in Fig. 1.   The panels show the 24-hour variations of three geomagnetic components (H: positive geomagnetic northward, D: positive eastward, and Z: positive downward) of Syowa magnetometer data, 1 kHz wave intensity, and 30 MHz CNA, respectively.   In the 1 kHz wave intensity, 0 dB corresponds to $10^{-33}\mathrm{T}^2/$ Hz.   The magnetic local time (MLT) at Syowa Station is approximately the same as the universal time (UT).   In the nighttime (before 06 UT and after 18 UT), strong geomagnetic disturbances (ΔH variations over several hundred nT) were observed, and the aurora-related particle precipitation and auroral hiss were observed on the CNA and VLF (1 kHz) wave intensity.   Similar onsets were clearly seen on all of the data in Fig. 1 at about 19 UT.

On the other hand, here we focus on the daytime variation (04 UT to 16 UT) of CNA and VLF waves, which seem to have a negative correlation between them.   In this study, we do not use the data at night, because we focus on the dayside chorus and the related particle precipitation.   The larger values of the CNA indicate more enhanced ionization of the ionospheric D-region, where the VLF emissions of magnetospheric origin would be strongly attenuated.   Thus, we would expect a negative correlation between the intensity of the VLF emissions and the CNA, which is caused by the electron precipitation associated with the pitch angle scattering by the VLF emissions.

Comparison between 1 kHz wave intensity of polar chorus and 30 MHz CNA during 04 UT to 16 UT is plotted in Fig. 2.   Different colors correspond to different time periods (Red: 04–07 UT, Green: 07–10 UT, Blue: 10–13 UT, and Magenta: 13–16 UT).   As expected, a negative correlation is observed above the CNA level of 0.3 dB.
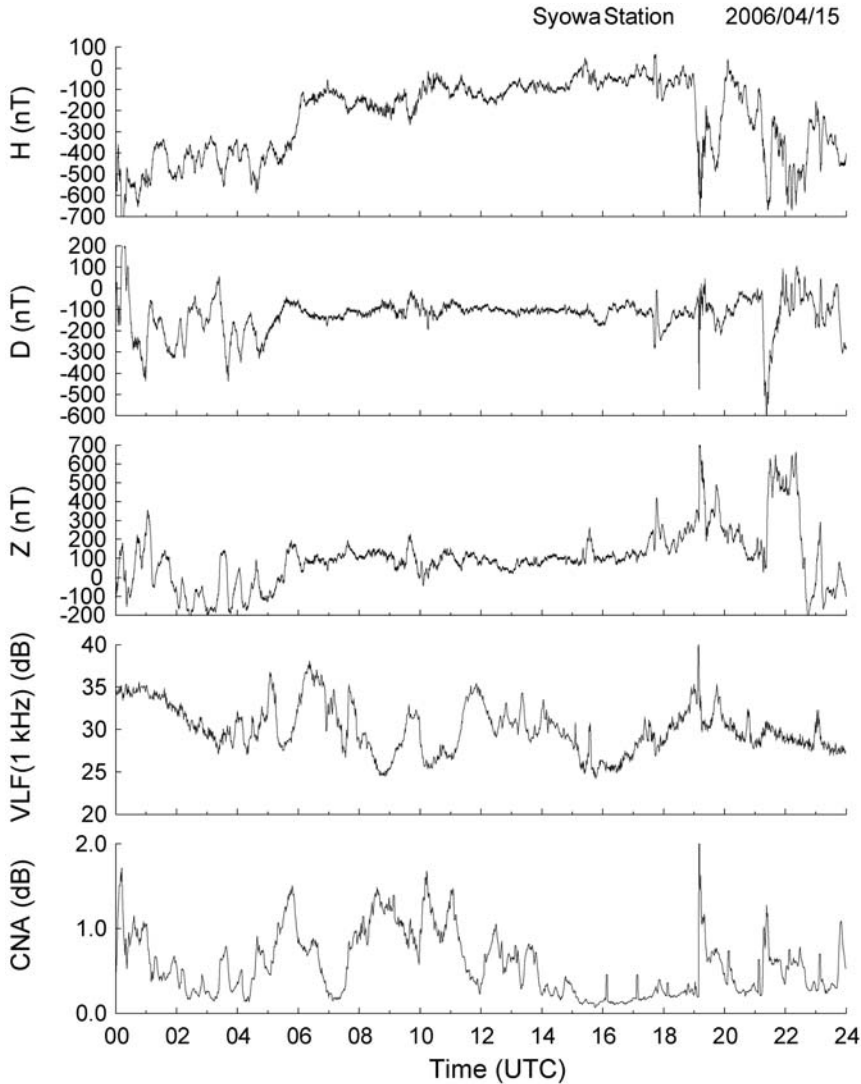
Fig. 1.   One-day profiles of the three components of geomagnetic variations, 1 kHz horizontal magnetic field intensity $(0\,dB = 10^{-33}T^2/Hz)$, and 30 MHz CNA observed on 15 April, 2006, at West Ongul (Syowa Station) (L-value: 6.2) in Antarctica.

In addition, we see a positive correlation for CNA less than 0.3 dB. The VLF emissions propagating down from the upper ionosphere can penetrate the lower ionosphere during small CNA.   However, as CNA gradually increases (indicating strong ionospheric absorption due to electron precipitation), the VLF emissions become strongly attenuated in the lower ionosphere.   Therefore, the CNA-VLF comparison exhibits both positive and negative correlations in this event.   From satellite observation, the VLF emission and particle precipitation would have a positive correlation (Miyoshi *et al*, 2003).   On the other hand, as mentioned above, they would have both
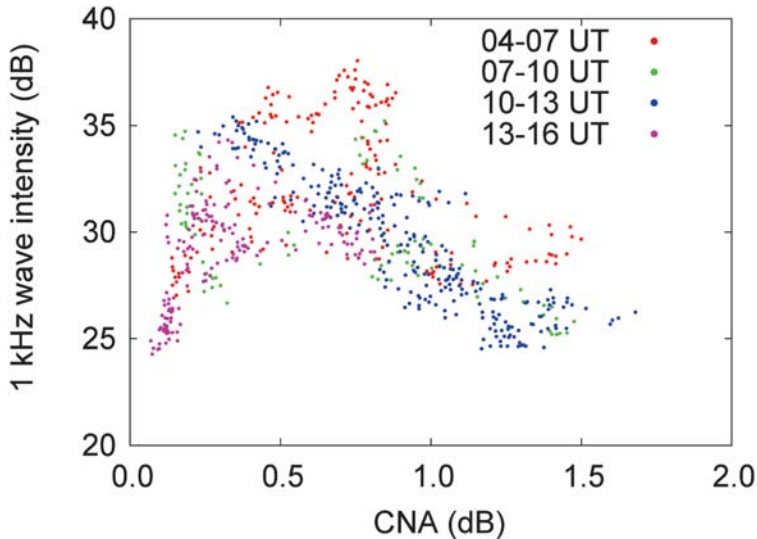
Fig. 2.   The CNA-VLF correlation during 04 UT to 16 UT on 15 April, 2006.

positive and negative correlations in the ground observations. Such a tendency is consistent with the previous work by Harang and Larsen (1965). Here, we can examine the negative CNA-VLF correlation by evaluating the wave attenuation at the two frequencies (CNA: 30 MHz and VLF: 1 kHz) in the ionospheric *D*-region. In the next section, the CNA-VLF correlation is theoretically calculated and evaluated with the enhanced electron density models.

3.   Full-Wave Analysis of the CNA-VLF Correlation

In order to theoretically estimate the CNA-VLF correlation, we calculate the 30 MHz and 1 kHz wave attenuation by using full-wave analysis. The computation code used here is based on the full-wave analysis for studying the VLF whistler mode plane wave propagation developed by Nagano *et al.* (1975). The ionospheric penetration of a 30 MHz plane wave can be easily calculated by using the WKB approximation, because the variation of the electron density in the lower ionosphere is relatively slow compared with the wavelength of 30 MHz (*e.g.*, Stauning, 1996). On the other hand, for the ionospheric penetration of a 1 kHz whistler mode plane wave, we cannot use the WKB approximation, instead we should use the full-wave analysis to rigorously calculate the ionospheric attenuation. The full-wave analysis has been successfully used in many works related to the ionospheric wave propagation and estimation of the electron density in the lower ionosphere by rocket experiments (*e.g.*, Nagano and Okada, 2000).

In this full-wave analysis, we use a one-dimensional calculation. The ionosphere is assumed to be a cold plasma medium, and vertically characterized by the electron density and the collision frequency between electrons and neutral particles. Full-wave analysis considers the effects of the inhomogeneous anisotropic ionosphere and of the direction and amplitude of the geomagnetic field line. The calculation algorithm is the

same as the one used in the full-wave analysis presented by Nagano *et al*. (1975), which incorporates mathematical techniques such as scaling down and orthogonalization to avoid numerical swamping caused by the evanescent mode (Pitteway, 1965).

The injected waves are assumed to be a 1 kHz whistler mode plane wave for the VLF emissions and as a 30 MHz plane wave for CNA, at the top layer (altitude 180 km) of the ionosphere with vertical incidence. For a usual electron density model, the vertically injected 30 MHz plane wave does not attenuate; it fully penetrates the lower ionosphere. When the lower ionosphere is abnormally ionized by particle precipitation, a 30 MHz plane wave slightly attenuates. In this study, we use the exponentially enhanced electron density model as follows,

$$N = N_0 \{1 + E_N \exp[-(z-z_0)^2/s_z^2]\}, \tag{1}$$

$$N_0 = 30.4 \exp[0.2(z-68.0)], \tag{2}$$

where N_0 is the background electron density, E_N is the enhancement factor for the electron density, and z is the altitude of the electron density profile. The parameters z_0 and s_z determine the altitude extent of the enhanced electron density. This model has been used for study of Trimpi events (Nunn *et al*., 1998). The electron density model above 100 km was calculated by the international reference ionosphere (IRI) model (Bilitza, 2001) and that below 100 km is based on the above enhanced electron density model. The effective electron-neutral particle collision frequency has been calculated to be proportional to both the neutral particle density and the electron temperature (Nicolet, 1953). In the lower ionosphere, the collision frequency between electrons and neutral particles dominates between electrons and ions. We calculate the ionospheric wave attenuation through an enhanced electron density model at the frequencies of 1 kHz and 30 MHz. The ionospheric wave attenuation at each frequency is defined as the ratio between the z component of the Poynting flux at the top ionospheric layer (altitude 180 km) and the one at the bottom layer (altitude 60 km).

At first, we make various enhanced electron density models, then we calculate the ionospheric attenuation of the 30 MHz plane wave (as the CNA value) with those models by using the full-wave analysis. Here, we plot the enhanced electron density models in the upper three panels of Fig. 3. The three panels are the electron density profiles for $z_0 = 85$, 80 and 75 km, respectively, and the four solid lines (electron density profiles) plotted in each panel give the CNA values of 0.5, 1.0, 1.5 and 2.0 dB. As it is generally known, the electron density increases with increasing CNA value. These panels also plot the original IRI model at noon on 15 April, 2006 as gray solid lines. The collision frequency is plotted as the dashed-dotted line. The other calculation parameters for evaluating CNA are: gyrofrequency is 1.208 MHz, geomagnetic inclination is 65.6 degrees, and $s_z = 10$ km. The maximum electron density in the models for $z_0 = 85$ km giving CNA $= 0.5$–2.0 dB occurs at altitude 95 km. To obtain the CNA $= 0.5$ and 2.0 dB, the electron densities at the altitude of 95 km are enhanced up to 1.16×10^5 and 4.68×10^5 electrons/cc from 0.19×10^5 electrons/cc in the IRI model. The altitude of maximum electron density goes down with decreasing z_0.

Next, the 1 kHz wave attenuation was calculated with the enhanced electron density model giving each CNA level. The theoretically calculated CNA-VLF relations
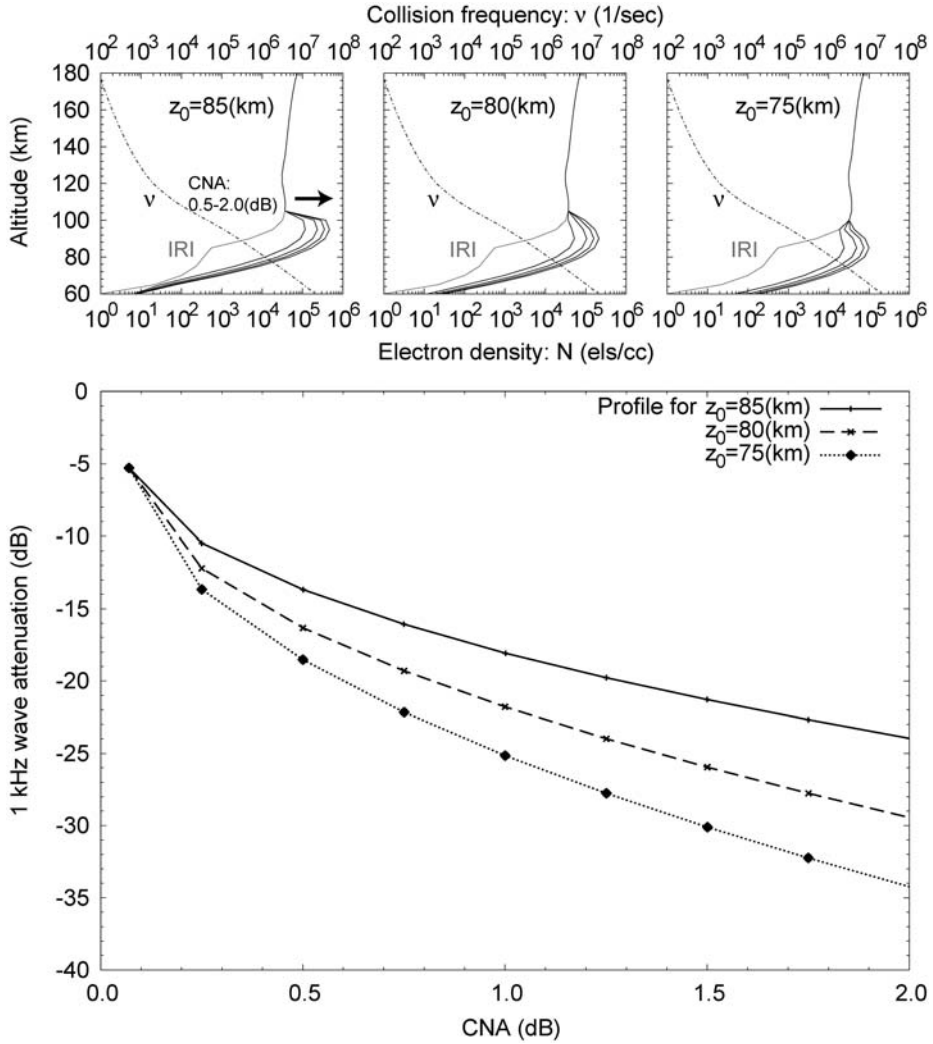
Fig. 3.   Effect on the CNA-VLF correlation of the parameter z_0. (upper three panels: The three panels are the electron density profiles for z_0=85, 80, and 75 km, and the four black solid lines (electron density profiles) plotted in each panel give the CNA values of 0.5, 1.0, 1.5 and 2.0 dB, respectively.   The gray solid line is the profile for the IRI model and the dashed-dotted line is the collision frequency.   Lower panel: the calculated CNA-VLF correlations with the above ionospheric models.)

are shown in the lower panel of Fig. 3 for different values of z_0.   All the calculated CNA-VLF relations look similar to the observed negative correlations shown in Fig. 2. The 1 kHz wave attenuation becomes -5 dB for the case of the IRI model (CNA=0.1 dB), while it gradually changes with increasing CNA and becomes -24 dB when CNA =2.0 dB for the case of the electron density model with z_0=85 km.   The most important point here is that the ionospheric wave attenuation at the VLF range is rigorously

calculated by the full-wave analysis.   The calculated CNA-VLF correlations with the different z_0 clearly have different negative gradients.   The negative gradient of CNA-VLF correlation becomes larger with decreasing parameter z_0.   Thus, we find an important consequence that the negative gradient of the CNA-VLF correlation gives information on the altitude enhanced of ionization in the lower ionosphere.

Here, the ionospheric wave attenuation at each altitude is proportional both to the electron density and to the collision frequency.   The collision frequency exponentially decreases with altitude, thus the electron density in the lower ionosphere mainly determines the ionospheric wave attenuation.   We found that the gradient of negative correlation between CNA and VLF emissions indicates the vertical extent of the enhanced electron density in the lower ionosphere during particle precipitation events. Therefore, we can inversely estimate the altitude profile of the electron density during the energetic particle precipitation by using observed information on wave attenuation at frequencies 1 kHz (VLF) and 30 MHz (CNA).

4.   Comparison between Observed and Calculated CNA-VLF Correlations

The observed CNA-VLF negative correlation during 10 to 13 UT on 15 April, 2006 in Fig. 2 is plotted again in Fig. 4 with the two lines of calculated correlations.   The calculated correlations are the profiles for the cases of $z_0 = 85$ and 80 km, which are found to almost fit the observations.   Here we assume that the intensities of VLF emissions in the magnetosphere stay constant to make the problem simple.   Because, in the VLF emission phenomena, the wave amplitude of the initial whistler mode wave could exponentially grow to a saturation level, which typically remains constant (Gibby *et al.*, 2008).   In this event, the observed correlations are scattered between the calculated lines for $z_0 = 85$ and 80 km.   Thus, we estimate that in this event the particles
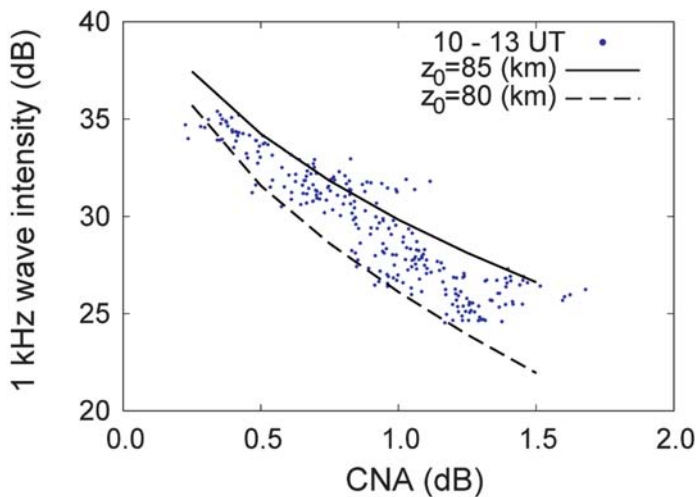
Fig. 4.   *Comparison between observed and calculated CNA-VLF*
correlations during 10 UT to 13 UT on 15 April, 2006.

precipitated down to altitude 95 to 90 km as shown in Fig. 3. Here, the enhancement altitude of the lower ionosphere implies the energy of the precipitating particles. Banks *et al.* (1974) calculated altitude profiles of ionization rates per unit incident particle flux. Their calculation results showed that the electrons at 0.8 keV can ionize the atmosphere above the altitude of 160 km, while the electrons at 10 keV can ionize and precipitate to the atmosphere around the altitude of 100 km. Thus, we may be able to even estimate the energies of the precipitated electrons from the enhanced electron density model, but it is beyond the scope of this study.

We obtained other interesting events, which have different gradients of CNA-VLF correlations. Fig. 5 shows the event on 22 March, 2006. The top panel is the 24-hour profiles of 30 MHz CNA and 1 kHz wave intensity, the middle panel is the observed and calculated CNA-VLF correlations, and the bottom panel is the ionospheric models used in the calculation, which gives the CNA = 0.5, 1.0 and 1.5 dB. In this CNA-VLF correlation, the positive and negative correlations are clearly observed. For the observed negative correlations during 6 to 12 UT (red and green dots), the theoretical CNA-VLF correlations were calculated with the various electron density models for different values of z_0. The most plausible result is plotted as the solid line in the middle panel of Fig. 5, with $z_0 = 71$ km. Similarly, the event on 10 April, 2006 is shown in Fig. 6. In this event, the negative correlation continued from 6 to 16 UT, then the calculation results in an electron density model with $z_0 = 85$ km, similar to the observation.

A number of previous have works reported electron precipitation associated with subionospheric VLF perturbations, as Trimpi events. Trimpi events are observed as rapid variations in the amplitude of long propagating subionospheric VLF waves only at **night**, They are caused by whistler- or ground-based VLF transmitter-induced electron precipitation into the lower ionosphere (*e.g.*, Helliwell *et al.*, 1973; Inan *et al.*, 1984). These events are not detected during the **daytime**. On the other hand, as shown above, we can obtain information on electron precipitation in the **daytime** by using the CNA and the natural VLF emissions with the full-wave analysis. We believe that this should be a significant advantage in studying electron precipitation from the radiation belt in the **daytime**.

5.   Conclusion

By comparing 30 MHz CNA and VLF emissions (1 kHz magnetic field intensity), we have investigated enhanced ionization in the lower ionosphere due to particle precipitation through pitch angle scattering by VLF emissions. We have found both the positive and negative correlations between them. Especially, we have focused on the negative correlations between 30 MHz CNA and VLF emissions, which are explained by the abnormal enhancement of electron density in the lower ionosphere.

Based on the calculated CNA-VLF correlations consistent with the observations, we have found that the gradients of their negative correlations indicate the vertical extent of the enhanced electron density. We could obtain information on electron density during particle precipitation events in the daytime, from the difference in the ionospheric attenuation at the two different frequencies (30 MHz and 1 kHz).
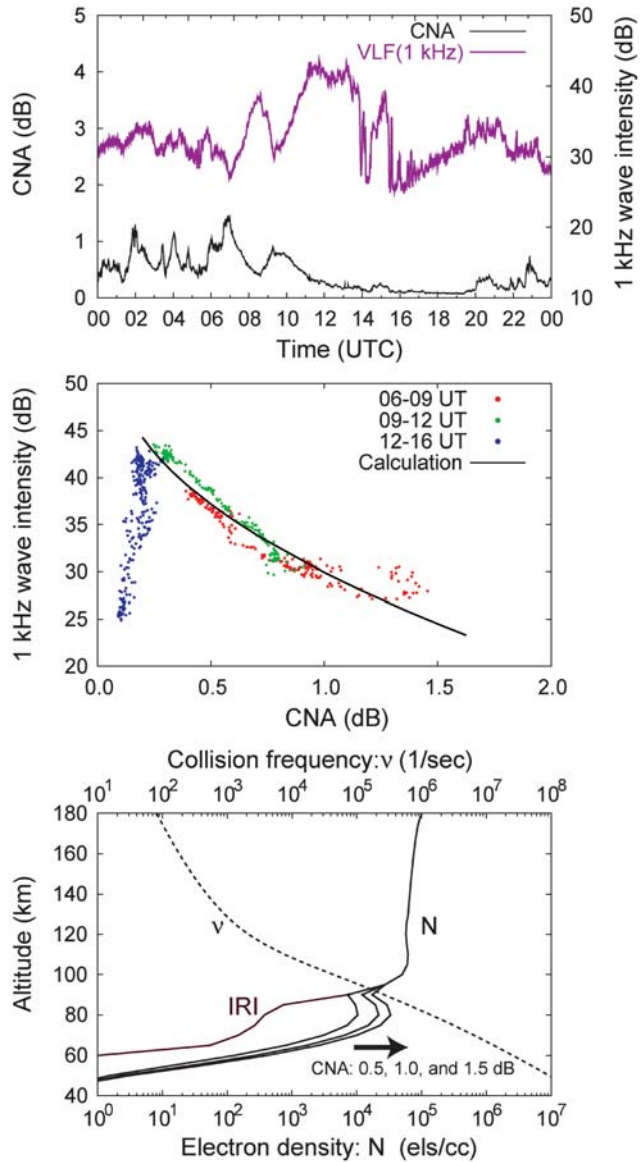
Fig. 5. *30 MHz CNA and 1 kHz wave intensity observed on 22 March, 2006 (top panel), their correlation (middle panel), and the collision frequency (dashed line) and the electron density models (solid lines) giving CNA = 0.5, 1.0 and 1.5 dB consistent with the calculation results (bottom panel).*

For investigation of the electron density in the ionosphere, several radar techniques such as ionosondes and incoherent scatter radars have been used. However, these radars do not work well for the ionospheric *D*-region (60–90 km). Rocket experiments can measure in-situ electron density in the *D*-region with Langmuir probes, but we cannot easily conduct rocket experiments. Thus, this present VLF and CNA remote
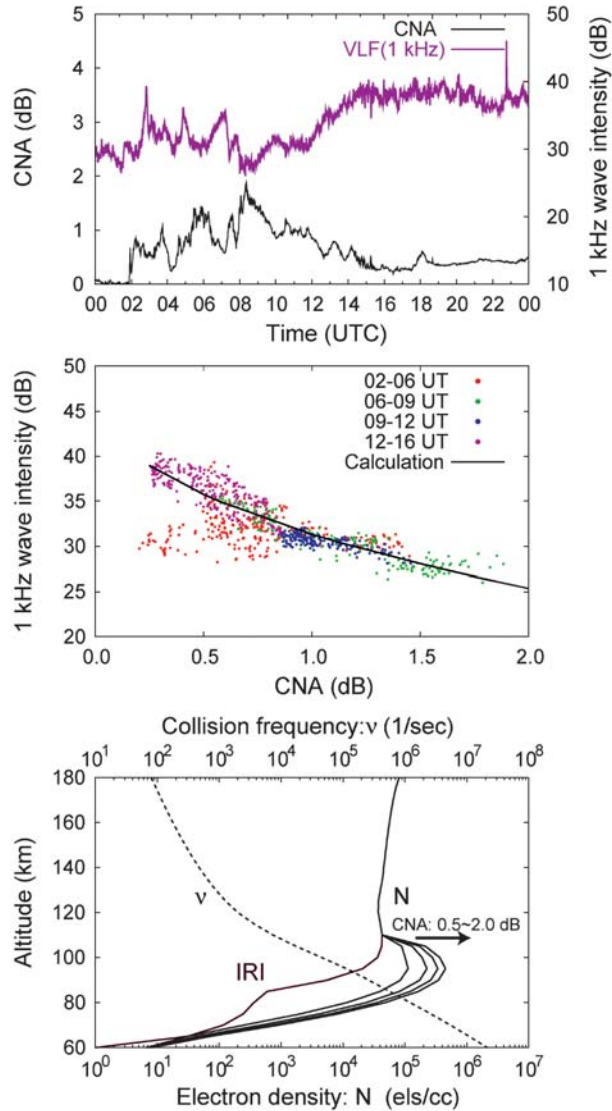
Fig. 6. *30 MHz CNA and 1 kHz wave intensity observed on 10 April, 2006 (top panel),
their correlation (middle panel), and the collision frequency (dashed line) and the
electron density models (solid lines) giving CNA=0.5–2.0 dB consistent with the
calculation results (bottom panel).*

sensing technique should be a useful tool for measuring electron density in the *D*-region.

   As a future work, we will compare the electron density estimated in this study with
in-situ electron density measurement.   Additionally, in order to evaluate the precipitat-
ing particle energy from the altitude profile of the enhanced electron density model, we
will investigate the relationship between ionization rates and particle energy by particle
simulation (*e.g.*, Banks *et al.*, 1974; Chang and Inan, 1985).   In this study, we assume

that the intensities of natural VLF emissions in the magnetosphere stay constant to make the problem simple. This assumption would be one of the major factors that increase the variance of CNA-VLF correlation. We should consider the intensities of magnetospheric VLF emissions in a more detailed analysis.

Clilverd *et al.* (2008) reported on a simulation study for a model of substorm electron precipitation by using riometer, subionospheric VLF signals (Trimpi events), and satellite particle data. Our full-wave techniques, natural VLF emissions, and riometer data could also support a modeling study for the substorm electron precipitation during the daytime in addition to the previous works using Trimpi events at night.

Acknowledgments

References

Banks, P.M., Chappell, C.R. and Nagy, A.F. (1974): A new model for the interaction of auroral electrons with the atmosphere: spectral degradation, backscatter, optical emission and ionization. J. Geophys. Res., **79**, 1459–1470.

Bilitza, D. (2001): International reference ionosphere 2000. Radio Sci., **36**, 261–275.

Collis, P.N. and Korth, A. (1985): GEOS-2 observations of energetic electrons in the morning sector during auroral radio absorption events. J. Atmos. Terr. Phys., **47**, 327–339.

Chang, H.C. and Inan, U. S. (1985): Test particle modeling of wave-induced energetic electron precipitation. J. Geophys. Res., **90**, 6409–6418.

Clilverd, M.A., *et al.* (2008): Energetic electron precipitation during substorm injection events: High-latitude fluxes and an unexpected midlatitude signature. J. Geophys. Res., **113**, A10311, doi: 10.1029/2008JA 013220.

Cummer, S.A., Bell, T.F., Inan U.S. and Chenette, D.L. (1997): VLF remote sensing of high-energy auroral particle precipitation. J. Geophys. Res., **102**, 7477–7484.

Gibby, A.R., Inan, U.S. and Bell, T.F. (2008): Saturation effects in the VLF-triggered emission process. J. Geophys. Res., **113**, A10311, doi: 10.1029/2008JA013233.

Harang, L. and Larsen, R. (1965): Radio wave emissions in the v.l.f.-band observed near the auroral zone — I occurrence of emissions during disturbances. J. Atmos. Terr. Phys., **27**, 481–497.

Helliwell, R.A., Katsufrakis J.P. and Trimpi, M.L. (1973): Whistler-induced amplitude perturbation in VLF propagation. J. Geophys. Res., **78**, 4679–4688.

Hoffman, R.A. and Laaspere, T. (1972): Comparison of very-low-frequency auroral hiss with precipitating low-energy electrons by the use of simultaneous data from two Ogo 4 experiments. J. Geophys. Res., **77**, 640–650.

Inan, U.S., Chang, H.C. and Helliwell, R.A. (1984): Electron precipitation zones around major ground-based VLF signal sources. J. Geophys. Res., **89**, 2891–2906.

Jelly, D. and Brice, N. (1967): Changes in Van Allen radiation associated with polar substorms. J. Geophys. Res., **72**, 5919–5931.

Miyoshi, Y., Morioka, A., Misawa, H., Obara, T., Nagai, T. and Kasahara, Y. (2003): Rebuilding process of the outer radiation belt during the 3 November 1993 magnetic storm: NOAA and Exos-D observations. J. Geophys. Res., **108**, (AI), 1004, doi: 10.1029/2001JA007542.

Nagano, I., Mambo, M. and Hutatsuishi, G. (1975): Numerical calculation of electromagnetic waves in an anisotropic multilayered medium. Radio Sci., **10**, 611–617.

Nagano, I. and Okada, T. (2000): Electron density profiles in the ionospheric D-region estimated from MF radio wave absorption, Adv. Space Res., **25**, 33–42.

Nicolet, M. (1953): The collision frequency of electrons in the ionosphere. J. Atmos. Terr. Phys., **3**, 200–211.

Nielsen, E. (1980): Dynamics and spatial scale of auroral absorption spikes associated with the substorm expansion phase. J. Geophys. Res., **85**, 2092–2098.

Nunn, D., Baba, K. and   Hayakawa, M. (1998): VLF Trimpi modelling on the path NWC-Dunedin using both finite element and 3D Born modelling. J. Atmos. Sol.-Terr. Phys., **60**, 1497–1515, doi: 10.1016/S 1364-6826(98)00088-1.

Pitteway, M.L.V. (1965): The numerical calculation of wave-fields, reflection coefficients and polarizations for long radio waves in the lower ionosphere. I. Philos. T. Roy. Soc. A, **257**, 219–241, doi: 10.1098/rsta. 1965.0004.

Rosenberg, T.J., Helliwell, R.A. and Katsufrakis, J.P. (1971): Electron precipitation associated with discrete very-low-frequency emissions. J. Geophys. Res., **76**, 8445–8452.

Stauning, P. (1996): Investigations of ionospheric radio wave absorption processes using imaging riometer techniques. J. Atmos. Terr. Phys., **58**, 753–764, doi: 10.1016/0021-9169(95)00072-0.